COBEM UBERLÂNDIA 2019

ABCM Associação Brasileira de Engenharia e Ciências Mecânicas

25th ABCM International Congress of Mechanical Engineering
October 20-25, 2019, Uberlândia, MG, Brazil

COB-2019-1580
TOPOLOGY OPTIMIZATION OF GEOMETRICALLY NONLINEAR STRUCTURES CONSIDERING AN ENERGY INTERPOLATION SCHEME

André Xavier Leitão
Anderson Pereira
Pontifical Catholic University of Rio de Janeiro, Marquês de São Vicente Street, 225, Gávea - Rio de Janeiro, RJ. Zip code: 22451-900
andrex.leitao@aluno.puc-rio.br
anderson@puc-rio.br

Abstract. *Topology optimization of geometrically nonlinear structures based on the finite element method suffers from numerical instabilities. This is caused by excessive distortions in low-density regions within the design domain which can jeopardize or even result in non-convergence of the optimization process. In this article, an interpolation scheme is studied to alleviate this convergence issue. The optimization is solved by the Method of Moving Asymptotes, that requires information on the gradients. These derivatives are computed employing the adjoint method. The Newton-Raphson approach is applied to determine the equilibrium points at each step of the solution during the optimization routine. Comparisons between two different nonlinear solution techniques are exhibited in the scope of the topology optimization method. Applicability and efficiency of this interpolation scheme are demonstrated by means of benchmark structures, which plays a crucial role in the geometric nonlinear analysis, allowing the optimization routine to converge and to obtain the optimal material arrangement.*

Keywords: *Topology Optimization, Geometric Nonlinearity, Finite Elements, Interpolation Scheme, Low-Density Elements*

1. INTRODUCTION

When structures undergo large deformations, the tangent stiffness matrix may no longer be positive definite. An easy way to comprehend this, is observing that large displacements can distort and flip some elements of the design domain into themselves, resulting in local material interpenetration. This is not evaluated by the classical Continuum Mechanics theory, in which the strain measures, based on the deformation gradient, has only physical meaning for bodies with positive volume. This phenomenon is known to happen in low-density (also called low-stiffness or void) elements of the domain due to large displacements of their nodal coordinates and it is said to be "artificial" since they should not influence the structural response (solid or high-stiffness elements). Nonetheless, the large displacement theory imposes difficulties or even results in non-convergence of the equilibrium iterations in the Newton-Raphson Procedure (NRP).

In the last two decades, several essays have appeared in the area of nonlinear optimization considering structures submitted to large displacements to solve specially the "end-compliance" minimization problem. To name a few: Bruns and Tortorelli (1998, 2001, 2003), Buhl *et al.* (2000), Kemmler *et al.* (2005), Pajot (2006), Lahuerta *et al.* (2013), Wang *et al.* (2014), Luo *et al.* (2015) and Chen *et al.* (2018).

Looking at the recent studies on the field of nonlinear geometric topology optimization, Lahuerta *et al.* (2013) investigated the neo-Hookean material law of Simo-Ciarlet. For design domains discretized by meshes of Q4 elements, which are more sensitive to mesh distortion, the neo-Hookean material model presented different results compared to the St. Venant-Kirchhoff (SVK) formulation in high load levels. Even though making use of hyperelastic model, the authors reported that numerical instabilities were not completely solved and the difficulties associated to large displacements were treated invoking a relaxation function.

Wang *et al.* (2014) suggested an energy interpolation scheme. The idea was to interpolate the strain energy density between the large and small deformations theories. Assuming, ideally, void regions have very small density, these areas can be modeled in any desired way so they will not influence the solid elements. Hence, the structural part was discretized according to the nonlinear premises and the low-density regions were modeled by the linear assumption.

Luo *et al.* (2015) formulated another interpolation scheme in which a model of hyperelastic material is added to the design domain. This approach has the great advantage of being easy to incorporate into commercial softwares, as recently done by Chen *et al.* (2018). The idea is to superimpose two distinct meshes: one discretized by elastic material, e.g. SVK, and another – the additive mesh – defined by the Yeoh model. To make this technique coherent, the design variables (densities) of the additive mesh must assume small values. By controlling the maximal von Mises strain, Luo *et al.* were

able to control the parameters of the additive mesh at each iteration of the optimization process. The authors reported the effectiveness of the technique to alleviate excessive distortions in low- and intermediate-density elements. A deeper look at this technique is needed, as it has not been proven that the approximation of the remodeled structure is sufficiently accurate.

To treat the stabilization issue in geometric nonlinear topology optimization and ensure its convergence, this paper studies an interpolation method based on the techniques of Pajot (2006) and Wang *et al.* (2014). For this purpose, the `PolyTop` framework by Talischi *et al.* (2012) is modified to include four-node-quadrilateral elements and it is extended to consider large displacements theory. The discussed method can be applied to the traditional SVK material law without the solution algorithm resulting in non-convergence of the optimization routine.

The equilibrium state is traced my means of the NRP (Leon *et al.*, 2011) and the Generalized Displacement Control Method (GDCM) from Yang and Shieh (1990). The Newton's method, also known as Load Control Method (LCM), imposes directly the load parameter (or load factor) $\delta\lambda$, which can be viewed as a fraction of the applied load. GDCM has the capability to change the load signal only at load limit points and the load factor can be adjusted according to the nonlinearities of the structure.

The outline of the paper is as follows: in Section 2, the topology optimization and its concepts are discussed. The optimization problem is properly defined here. The Section 3 formally introduces the formulation to alleviate numerical instabilities associated to void elements. In Section 4, a brief review on finite element analysis focused on the studied technique is presented. The Section 5 is regarded to illustrate the results for the cantilever beam and the clamped beam considering the investigated scheme. The brief comparison between LCM and GDCM is discussed for the cantilever beam example. The Section 6 is about the conclusions from the accomplished results.

2. TOPOLOGY OPTIMIZATION

The goal of topology optimization method (Bendsøe and Kikuchi, 1988) is to determine the best material distribution Ω_s of a physical system. Typically, one defines a design domain Ω, where the boundary $\partial\Omega$ is divided into a portion Γ_D over which the displacements are prescribed and the remainder is either free or subject to imposed traction $\boldsymbol{t}$, cf. Fig. 1. The amount of eliminated material in the domain is $\Omega_v = \Omega \backslash \Omega_s$.

A common approach, by computational means, is to discretize the design domain by finite elements. The design variable z_e is attributed to each element of the mesh and it can assume values of 0 for voids or 1 for structural elements. However, the discrete formulation results in an ill-posed problem. So, the formulation is relaxed and each design variable is assumed to varies in the range $[0, 1]$. As consequence, gradient-based optimizers, such as the Method of Moving Asymptotes (MMA) from Svanberg (1987), can be applied. A regularization scheme, e.g. filter (see Section 2.1), enforces well-posedness of the optimization problem.

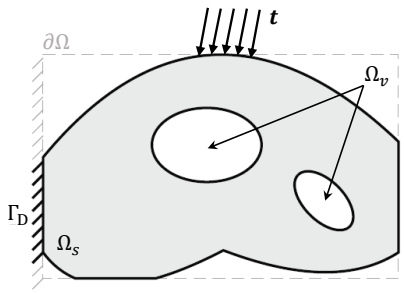

Figure 1. Representative design domain Ω of a topology optimization problem

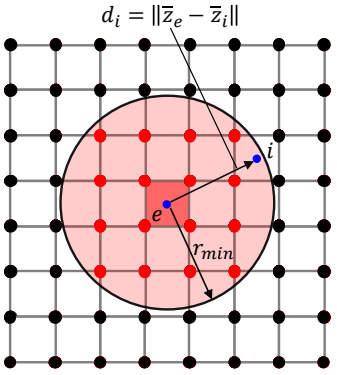

Figure 2. Top view of linear filter

2.1 Linear Filter

Filters make the problem well-posed, prevent the appearance of checkerboards and avoid mesh-dependency (Bendsøe and Sigmund, 2003). The design variable or density filter (Bruns and Tortorelli, 2001) acts directly modifying the density of a certain element z_e based on the weighted average densities in the neighborhood. It allows local control on material distribution and ensures a smooth transition of the density field. For the discrete case and $\overline{z}_e$ representing the centroid of the eth element, the equation for this filter is

$$y_e = \frac{\sum\limits_{i \in N_e} w_i\left(\overline{z}_e, \overline{z}_i\right) z_i}{\sum\limits_{i \in N_e} w_i\left(\overline{z}_e, \overline{z}_i\right)}, \tag{1}$$

where y_e is the "filtered" design variable, $\overline{z}_i$ is the location of the ith design variables and N_e is the number of elements in the design domain Ω. The weight distribution function w is

$$w_i\left(\overline{z}_e, \overline{z}_i\right) = max\left(1 - \frac{d_i}{r_{min}},\ 0\right), \tag{2}$$

for d_i being the (Euclidean) distance from element e to element i: $d_i = ||\overline{z}_e - \overline{z}_i||_2$. The filter radius r_{min} is previously defined according to the average size of elements in the mesh and kept constant in the optimization process.

Equation (1) can be written in matrix form, which is very helpful to deduce the derivatives of the objective (see Section 3.1),

$$\boldsymbol{y} = \boldsymbol{M}\boldsymbol{z}, \tag{3}$$

on what $\boldsymbol{z}$ is the vector of design variables, $\boldsymbol{y}$ is the corresponded "filtered" vector and $\boldsymbol{M}$ is the matrix of weight indexes defined by

$$M_{ei} = \frac{w_i\left(\overline{z}_e, \overline{z}_i\right)}{\sum\limits_{i \in N_e} w_i\left(\overline{z}_e, \overline{z}_i\right)}.$$

This filter is also known as linear hat kernel since the weight function decays linearly with the distance from element e: it has magnitude 1 at the element centroid and 0 at r_{min} similar to a birthday party hat in three-dimensional analysis. The top view of the filter is illustrated in Fig. 2.

2.2 Solid Isotropic Material with Penalization (SIMP)

Continuous approach introduces intermediate values of the design variable. In general, these values have no physical meaning, as the method was originally formulated to represent isotropic materials (Bendsøe, 1989). Therefore, the design variables should be penalized to recover the discrete characteristic. A popular method is the SIMP, Solid Isotropic Material with Penalization (Bendsøe and Sigmund, 2003):

$$\tilde{x}_e(y_e) = \epsilon + (1 - \epsilon)g(y_e)^p, \quad \text{for} \quad p \geqslant 1, \tag{4}$$

where ϵ is the Ersatz parameter (a small positive number, e.g. 10^{-4}) to ensure non-singularities when the function $g(y_e) \to 0$. The exponent p is the penalization parameter and $\tilde{x}_e$ is the material interpolation function.

Most topology optimization problems are non-convex and the solution may not achieve the global minimum point. A technique called continuation scheme can be implemented to avoid the optimization to converge to an undesirable local solution (Sigmund and Petersson, 1998). The idea is to gradually increase the exponent p by an increment Δp,

$$p_{i+1} = p_i + \Delta p, \tag{5}$$

starting from $p = 1$ to a certain limit, typically $p = 3$. Thus, an optimization problem is solved for each p_i.

2.3 Nonlinear Projection Function

Wang *et al.* (2011) showed the gray tones can be significantly reduced from the optimized layout evoking nonlinear functions, as the hyperbolic tangent $\tanh$. In short, it is possible to couple the $\tanh$-projection function,

$$\overline{y}_e(y_e) = \frac{\tanh\left(\beta\eta\right) + \tanh\left(\beta\left(y_e - \eta\right)\right)}{\tanh\left(\beta\eta\right) + \tanh\left(\beta\left(1 - \eta\right)\right)}, \tag{6}$$

to the SIMP approach at certain iterations of continuation. The function $g(y_e)$ in Eq. (4) is properly defined as

$$g(y_e) = \begin{cases} y_e, & \text{for SIMP method} \\ \overline{y}_e, & \text{for projection function.} \end{cases}$$

That means one can choose whether to apply the SIMP method or the $\tanh$-projection function. Yet, it is strongly recommended to adopt this projection function at the very ending of the optimization process. This occurs because the $\tanh$ function tends to be very aggressive and it rapidly modifies the elements' behavior. Some analyses in this paper consider the SIMP method ($g = y_e$) in the material interpolation function during continuation, except for the last exponent, set to $p = 3$, where the $\tanh$ function ($g = \overline{y}_e$) is evoked, and the elements' behavior was already stabilized. In other examples, only the SIMP is implemented.

2.4 Optimization Problem

The optimization problem is the minimization of "end-compliance" c:

$$\min_{\boldsymbol{z}} \quad c = \boldsymbol{l}^T \boldsymbol{u} \tag{7a}$$

$$\text{s.t.:} \quad \sum_{e=1}^{N_e} V_e \leqslant V^* \tag{7b}$$

$$0 \leqslant \boldsymbol{z} \leqslant 1 \tag{7c}$$

$$\text{with} \quad \boldsymbol{r}(\boldsymbol{z}, \boldsymbol{u}) = \boldsymbol{l}(\boldsymbol{u}) - \boldsymbol{f}(\boldsymbol{z}, \boldsymbol{u}) \approx \boldsymbol{0}. \tag{7d}$$

The objective is defined by Eq. (7a), where $\boldsymbol{l}$, $\boldsymbol{f}$ and $\boldsymbol{u}$ are, respectively, the vectors of external and internal forces and displacements. Equation (7b) restricts the amount of allowed material in the optimal solution by controlling the amount of allowed volume V^*. It is a common practice to define the ratio between the allowed and initial volumes: $V_{frac} = V^*/V_0$. Equation (7c) limits the design variable range and the relation in Eq. (7d) is the structural equilibrium, where $\boldsymbol{r}$ is the residual force vector.

3. MODELING OF VOID ELEMENTS

As the source of the numerical instabilities are associated to large displacements, Pajot (2006) proposed a simply interpolation scheme, based on remodeling the kinematic relations. Therefore, the element residual force $\boldsymbol{r}_e$ was written as a combination of linear and nonlinear terms:

$$\boldsymbol{r}_e = \gamma_e^h \boldsymbol{r}_e^{NL} + (1 - \gamma_e^h)\boldsymbol{r}_e^L, \quad 0 \leqslant \gamma_e^h \leqslant 1, \tag{8}$$

for γ_e^h being the homotopic parameter,

$$\boldsymbol{r}_e^L = \boldsymbol{l}_e - \boldsymbol{f}_e^L \quad \text{and} \quad \boldsymbol{r}_e^{NL} = \boldsymbol{l}_e - \boldsymbol{f}_e^{NL}, \tag{9}$$

where $\boldsymbol{l}_e$ is the element external force vector and $\boldsymbol{f}_e^L$ and $\boldsymbol{f}_e^{NL}$ are, respectively, the linear and nonlinear terms of the element internal force vector.

Nevertheless, Wang *et al.* (2014) observed, when elements undergo large deformations, that approach can still result in numerical instabilities, such as the negative determinant of the deformation gradient J. So, the authors studied a different interpolation. Conceptually, if modeled by sufficiently low-density, void elements do not influence the structural parts of the domain. With this concept in mind, the strategy, named energy interpolation scheme, interpolates the stored elastic energy density function ϕ according to

$$\phi_e\left(\boldsymbol{u}_e\right) = \left[\phi\left(\gamma_e \boldsymbol{u}_e\right) - \phi_L\left(\gamma_e \boldsymbol{u}_e\right) + \phi_L\left(\boldsymbol{u}_e\right)\right] E_{0e}, \tag{10}$$

on what E_{0e} and $\boldsymbol{u}_e$ are, respectively, the Young's modulus and the vector of displacements of element e. The variable ϕ is the stored elastic energy density function for the base material with unit Young's modulus, ϕ_L is the stored elastic energy density under small deformations also with $E_{0e} = 1$ and γ_e is the interpolation factor.

One can observe for solid elements, $\gamma_e = 1$, the element stored elastic energy is $\phi_e = \phi\left(\boldsymbol{u}_e\right) E_{0e}$. This means, those elements are modeled according to the large deformation theory. For void elements, $\gamma_e = 0$, the stored elastic energy depends only on its linear term: $\phi_e = \phi_L\left(\boldsymbol{u}_e\right) E_{0e}$. Therefore, voids are modeled according to the linear strain energy theory ϕ_L and required to have small deformations. In turn, the structural elements are described by the nonlinear theory.

The interpolation factor γ_e for the continuous case must be aggressive, close to Heaviside function, smooth and differentiable to properly represent the element's behavior (small or large deformations). Hence,

$$\gamma_e(\tilde{x}_e) = \frac{\tanh\left(\alpha\rho\right) + \tanh\left(\alpha\left(\tilde{x}_e - \rho\right)\right)}{\tanh\left(\alpha\rho\right) + \tanh\left(\alpha\left(1 - \rho\right)\right)}, \tag{11}$$

where α controls the sharpness of the interpolation factor, ρ is a threshold parameter to define the element's behavior and $\tilde{x}_e$ correspond to the design variable after it has been "filtered" and penalized (Sections 2.1 and 2.2). It is worth to point out that these variables are different from those in Eq. (6), despite of both being modeled by the same function.

The sharpness α must assume a higher value to guaranty a smooth transition between linear and nonlinear cases. The concerning variable is ρ: it should not be too low nor too high. Low values ($\rho \to 0$) will impose linear behavior on the elements, what does not reproduce the mechanics of the problem. Besides, for the high ones, the elements will be characterized by large displacements and the distortions of voids may recover the numerical instabilities, which may result

in non-convergence of optimization. Wang *et al.* (2014) suggests $\alpha = 500$ and $\rho = 0.01$ and those values are adopted in all examples conducted in Section 5.

For the density-based approach of topology optimization, the design variables are continuous. Inspired by Pajot's formulation and considering the interpolation factor of Eq. (11), the following interpolation strategy is adopted:

$$\boldsymbol{K}_e = \tilde{x}_e \left[\boldsymbol{K}_e^{NL} \gamma_e + (1 - \gamma_e) \, \boldsymbol{K}_e^{L} \right]; \tag{12}$$

$$\boldsymbol{f}_e = \tilde{x}_e \left[\boldsymbol{f}_e^{NL} \gamma_e + (1 - \gamma_e) \, \boldsymbol{f}_e^{L} \right], \tag{13}$$

in which $\boldsymbol{K}_e$ and $\boldsymbol{f}_e$ are, respectively, the tangent stiffness matrix and the internal force vector of element e. The matrices $\boldsymbol{K}_e^L$, $\boldsymbol{K}_e^{NL}$, $\boldsymbol{f}_e^L$ and $\boldsymbol{f}_e^{NL}$ are introduced in Section 4.

3.1 Sensitivity Analysis

The sensitivity analysis is a fundamental part of topology optimization, since it uses gradient-based solvers. Assuming the equilibrium is reached at the end of each solution step of the incremental-iterative analysis, the residual force vector $\boldsymbol{r}$ is zero and Eq. (7a) can be rewritten as a function of the adjoint vector $\boldsymbol{\psi}$:

$$c = \boldsymbol{l}^T \boldsymbol{u} + \boldsymbol{\psi}^T \boldsymbol{r}. \tag{14}$$

As the displacement vector $\boldsymbol{u}$ depends on the design variable z_e, the sensitivity of Eq. (14) becomes

$$\frac{dc}{dz_e} = \boldsymbol{l}^T \frac{\partial \boldsymbol{u}}{\partial z_e} + \boldsymbol{\psi}^T \left(\frac{\partial \boldsymbol{r}}{\partial z_e} + \frac{\partial \boldsymbol{r}}{\partial \boldsymbol{u}} \frac{\partial \boldsymbol{u}}{\partial z_e} \right) = \left(\boldsymbol{l}^T - \boldsymbol{\psi}^T \boldsymbol{K} \right) \frac{\partial \boldsymbol{u}}{\partial z_e} + \boldsymbol{\psi}^T \frac{\partial \boldsymbol{r}}{\partial z_e}, \tag{15}$$

where

$$\frac{\partial \boldsymbol{r}}{\partial \boldsymbol{u}} = -\frac{\partial \boldsymbol{f}}{\partial \boldsymbol{u}} = -\boldsymbol{K}. \tag{16}$$

To determine $\partial c / \partial z_e$, the first term on the right-hand side of Eq. (15) should vanish. Since there is no restriction regarding the adjoint vector, the natural choice is to admit

$$\boldsymbol{\psi} = \boldsymbol{K}^{-1} \boldsymbol{l} \tag{17}$$

and Eq. (15) becomes

$$\frac{dc}{dz_e} = -\boldsymbol{\psi}^T \frac{\partial \boldsymbol{f}}{\partial z_e}. \tag{18}$$

The derivative of the internal force is calculated by the following chain rule over the N_e elements of the design domain:

$$\frac{\partial \boldsymbol{f}}{\partial z_e} = \sum_{j=1}^{N_e} \left(\frac{\partial \boldsymbol{f}_j}{\partial \tilde{x}_j} + \frac{\partial \boldsymbol{f}_j}{\partial \gamma_j} \frac{\partial \gamma_j}{\partial \tilde{x}_j} \right) \frac{\partial \tilde{x}_j}{\partial y_j} \frac{\partial y_j}{\partial z_e}, \tag{19}$$

where

$$\frac{\partial y_j}{\partial z_e} = M_{je}, \tag{20}$$

$$\frac{\partial \tilde{x}_j}{\partial y_j} = p(1 - \epsilon) g(y_j)^{p-1} \frac{\partial g}{\partial y_j}, \tag{21}$$

for the matrix $\boldsymbol{M}$ defined in Eq. (3), $g(y_j)$ given by Eq. (6) and

$$\frac{\partial g}{\partial y_j} = \begin{cases} 1 & \text{for SIMP method} \\ \dfrac{\beta \operatorname{sech}^2(\beta(y_j - \eta))}{\tanh(\beta(1 - \eta)) + \tanh(\beta \eta)} & \text{for tanh projection function} \end{cases} \tag{22}$$

The derivative of the interpolation factor γ_j is

$$\frac{\partial \gamma_j}{\partial \tilde{x}_j} = \frac{\alpha \operatorname{sech}^2(\alpha(\tilde{x}_j - \rho))}{\tanh(\alpha(1 - \rho)) + \tanh(\alpha \rho)}. \tag{23}$$

The derivative of internal force $\boldsymbol{f}_j$ is described by

$$\frac{\partial \boldsymbol{f}_j}{\partial \tilde{x}_j} = \frac{\partial}{\partial \tilde{x}_j} \left[\left(\gamma_j \boldsymbol{f}_j^{NL} + (1 - \gamma_j) \, \boldsymbol{f}_j^{L} \right) \tilde{x}_j \right] = \gamma_j \boldsymbol{f}_j^{NL} + (1 - \gamma_j) \, \boldsymbol{f}_j^{L} \tag{24}$$

and

$$\frac{\partial \boldsymbol{f}_j}{\partial \gamma_j} = \tilde{x}_j \left(\boldsymbol{f}_j^{NL} - \boldsymbol{f}_j^{L} \right). \tag{25}$$

4. FINITE ELEMENT EQUATIONS

The finite element theory (for SVK material law) is based on Bathe (2014). The equilibrium of Eq. (7d) is solved according to incremental-iterative methods (Leon *et al.*, 2011) which results in

$$\boldsymbol{K}\delta\boldsymbol{u} = \boldsymbol{r}, \tag{26}$$

where the tangent stiffness matrix is

$$\boldsymbol{K} = -\frac{\partial \boldsymbol{r}}{\partial \boldsymbol{u}}. \tag{27}$$

The element stiffness matrix $\boldsymbol{K}_e$ under small deformation theory is

$$\boldsymbol{K}_e^L = \int_{\Omega_e} \boldsymbol{B}_{L0}^T \boldsymbol{D}^0 \boldsymbol{B}_{L0}\, \mathrm{d}V \tag{28}$$

and for large deformations is

$$\boldsymbol{K}_e^{NL} = \int_{\Omega_e} \left[\left(\boldsymbol{B}_{L0} + \boldsymbol{B}_{L1}\right)^T \boldsymbol{D}^0 \left(\boldsymbol{B}_{L0} + \boldsymbol{B}_{L1}\right) + \boldsymbol{B}_{NL}^T \hat{\boldsymbol{S}} \boldsymbol{B}_{NL} \right] \mathrm{d}V \tag{29}$$

where $\boldsymbol{D}^0$ is the matrix representation of the elasticity tensor (without any penalization), $\hat{\boldsymbol{S}}$ is the expanded matrix of the 2nd Piola-Kirchhoff stress tensor $\boldsymbol{S}$ and $\boldsymbol{B}_{L0}$, $\boldsymbol{B}_{L1}$ and $\boldsymbol{B}_{NL}$ are the deformation-displacement matrices. The internal force vector $\boldsymbol{f}_e$ regarding only small deformations is

$$\boldsymbol{f}_e^L = \int_{\Omega_e} \boldsymbol{B}_{L0}^T \boldsymbol{D}^0 \boldsymbol{B}_{L0} \boldsymbol{u}_e\, \mathrm{d}V \tag{30}$$

and for large deformations the internal force vector is function of the vector of stresses $\overline{\boldsymbol{S}}$:

$$\boldsymbol{f}_e^{NL} = \int_{\Omega_e} \left(\boldsymbol{B}_{L0} + \boldsymbol{B}_{L1}\right)^T \overline{\boldsymbol{S}}\, \mathrm{d}V. \tag{31}$$

For more details about these matrices and the finite element formulation itself, one should go to Bathe (2014) among other classical readings.

5. RESULTS

To verify the application of the interpolation scheme defined in Section 3, two structures are considered: the cantilever beam and the clamped beam (Buhl *et al.*, 2000). All studies are conducted for a plane strain state, considering, as the objective function, the "end-compliance" at the load application point, cf. Eq. (7a). Different load levels are investigated for the same structure and the nonlinear state equation is solved using the LCM at each step of the optimization. The implemented algorithm always ensures that the external load reach its maximum value during the optimization process. The MMA optimizer is chosen to solve the topology optimization problem.

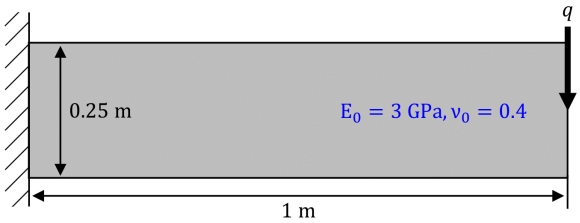

Figure 3. Cantilever beam

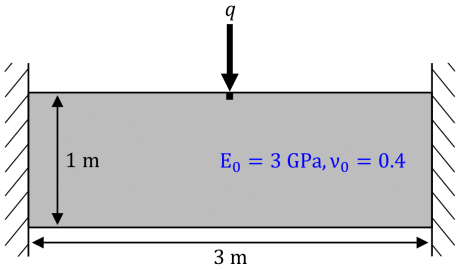

Figure 4. Clamped beam

5.1 Cantilever Beam

The cantilever beam, cf. Fig. 3, is 1 m long (b), 0.25 m height (h) and 0.1 m deep (d). The Young's modulus E_0 is 3 GPa and the Poisson's coefficient ν_0 is 0.4. This model is fixed on the left edge and loaded downwards at the midpoint of the right edge by the force $\boldsymbol{q}$. The domain is modeled by 120 x 30 Q4 elements and the volume fraction is $V_{frac} = 0.5$.

The penalization factor starts at $p = 1$ and is increased by $\Delta p = 0.05$ until it reaches a maximum value of 3. The same procedure adopted by Wang *et al.* (2014) is considered here: until $p < 2$ the optimization iterations are restricted to 2; from $2 \leqslant p < 3$, a maximum of 5 iterations are allowed. When $p = 3$, the optimization process stops only if it converges or reaches the maximum iterations allowed $Iter_{max} = 200$. The filter radius is $r_{min} = h/8$.

The SIMP method is employed until $p = 3$, then the $\tanh$-projection function is combined with it, as discussed in Section 2.3; β starts from an initial value of 4 and is doubled every 10 iterations until it reaches a maximal value of 64. In this manner, the routine allows the interpolation scheme to establish well-defined behaviors for each element in the domain before the projection function modifies the element densities. And more, it plays a crucial role reducing the compliance value as it diminishes the grayish of the optimal geometry. Not combining (nonlinear) projection functions to SIMP will result in similar structures, but the large presence of intermediate densities in their layouts tends to make the final topology stiffer than presented here.

The solution of the linear and nonlinear analyses are known to be different from each other, due to the loss of symmetry that is induced when large displacements are considered in the finite element formulation, modifying the sensitivities and consequently the design variable. In a previous work (Leitão and Pereira, 2018), it was shown that applying the proposed interpolation scheme result in similar topologies to those obtained assuming nonlinear behavior only. Furthermore, this scheme enables to achieve the optimal topology for high levels of load, as 240 and 300 kN, which the algorithm was not capable to determine without this interpolation method. The optimal layouts, by means of the interpolation strategy, are printed out in Fig. 5 for initial load factor $\delta\lambda_0 = 0.05q$.

Figure 6 illustrates the structural deformation of the beam displayed in Fig. 5(f) when the low-density elements are eliminated from the design domain. As expected the compliance is very close to each other, which demonstrates the efficiency of the optimization code as it reduces most of intermediate densities from the final layout.

(a) $q = 12$ kN, $c = 0.1469$ kJ

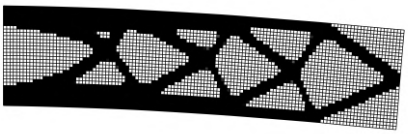

(b) $q = 60$ kN, $c = 3.6702$ kJ

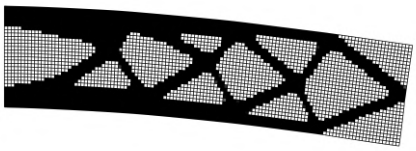

(c) $q = 96$ kN, $c = 9.3525$ kJ

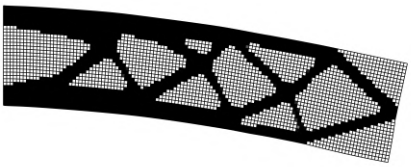

(d) $q = 144$ kN, $c = 20.8792$ kJ

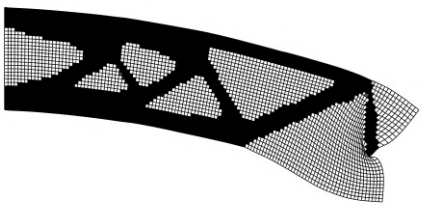

(e) $q = 240$ kN, $c = 56.3350$ kJ

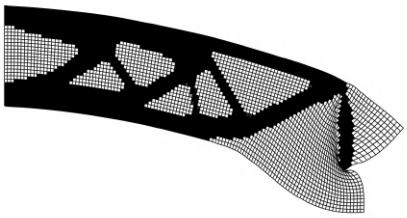

(f) $q = 300$ kN, $c = 84.8276$ kJ

Figure 5. Optimal topologies and corresponded compliance c obtained via interpolation scheme for the cantilever beam problem at several load levels

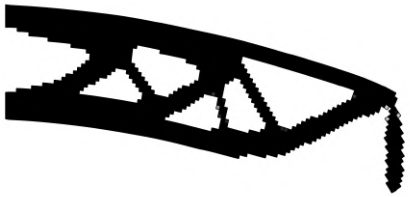

Figure 6. Structural deformation of the structure in Fig. 5(f) without void regions. The compliance c is 84.8309 kJ

Most of geometric nonlinear topology optimization analysis is conducted by LCM to determine the equilibrium points. To verify the effect of considering other nonlinear solution approaches, the GDCM is applied to the cantilever beam

problem. Figure 7 shows the effect of varying the initial prescribed load factor $\delta\lambda_0$ by employing the LCM or the GDCM. These graphs consider the applied force $q = 240$ kN and the convergence criterion for the nonlinear (NL) solution method is the norm of the iterative displacement $||\delta \boldsymbol{u}|| = 10^{-3}$. The abscissa indicates the number of topology optimization (TO) iterations; on the left y-axis is the number of iterations of the NL solution method and on the right y-axis is the value of the objective function, Eq. (7a).

In all cases, there are points with high number of iterations. This is directly associated to the distortions of low-stiffness regions as the elements are not yet sufficiently penalized at that stage of the optimization process. For such cases, the GDCM seems to be a better option as it reduces the number of total iterations. However, this method can be more sensitivity to numerical instabilities, as indicated in Fig. 7(c), where the objective function grows rapidly at the 153rd iteration. What could explain this effect is the emergence of void elements that present large displacements. On subsequent iterations, the objective returns to its expected behavior after these voids were modified by the interpolation scheme. For all other load factors, the "end-compliance" has the common behavior encountered in topology optimization routines that employ continuation. Concerning the optimal layout, for the different $\delta\lambda_0$ explored, very similar topologies to those in Fig. 5 were attained.

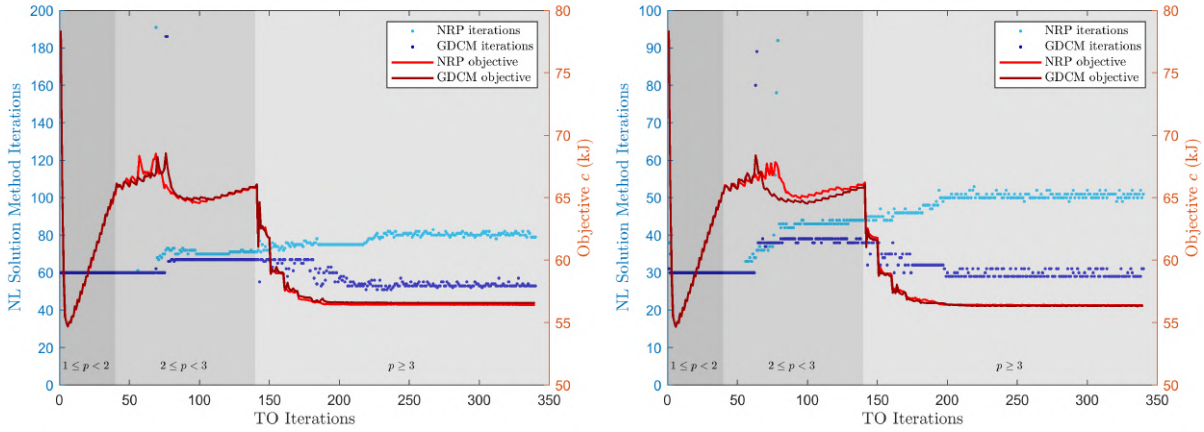

(a) Initial load factor $\delta\lambda_0 = 0.05q$

(b) Initial load factor $\delta\lambda_0 = 0.1q$

(c) Initial load factor $\delta\lambda_0 = 0.25q$

(d) Initial load factor $\delta\lambda_0 = 0.5q$

Figure 7. Influence of $\delta\lambda_0$ in the optimization process for two NL solution methods and an applied load $q = 240$ kN

5.2 Clamped Beam

The clamped beam (Buhl *et al.*, 2000) is fixed on both sides and the force (of magnitude q) is applied at the midpoint on the upper edge, as shown in Fig. 4. The geometry is b x h x d = 3 m x 1 m x 0.1 m, the Young's modulus E_0 and the Poisson's coefficient ν_0 are, respectively, 3 GPa and 0.4. The design domain is discretized by 120 x 40 Q4 elements and the allowed volume V^* is set to be 10% of the initial volume V_0.

This structure exhibits large distortions in elements around the load application point, due to small percentage of allowed material. To relax the mesh distortion in the vicinity of loading point, the force is uniformly distributed over the nodes of four adjacent elements, as indicated by the black square box below the load application point. This is a common practice in the literature, e.g. Luo *et al.* (2015).

The same continuation strategy for the cantilever beam is adopted in this example, except by the increment Δp, which is set to 0.1. A different strategy to reduce the gray tones on the final layout is considered in this example. At the end of optimization, the filter influence is eliminated. In short, the optimization process is conducted via the SIMP method and the linear filter for a radius $r_{min} = h/20$. Then, another analysis is run (considering the basis of `PolyTop` framework) without filter until the solution converges.

For the load of 230 kN, the above strategy leads to the topologies displayed in Fig. 8(a) and in Fig. 8(b) considering, respectively, the small deformation theory and the investigated interpolation scheme. The difference in the optimal layout is notable and the compliance also contrasts: it is 5.7417 kJ in the linear analysis and 11.9446 kJ when the elements' behavior are interpolated.

Assuming that the optimal structure of Fig. 8(a) is submitted to large displacements will result in the deformed structure of Fig. 8(c). One can observe this layout is too softer (the compliance is two-order higher from the optimal linear solution) and results in an undesired deformed configuration. Hence, it must be set aside in detriment of the topology of Fig. 8(b), that is correctly optimized regarding geometric nonlinearities and has the deformed shape printed in Fig. 8(d). When low-stiffness elements are eliminated from the domain the compliance is a little bit smaller 11.9261 kJ.

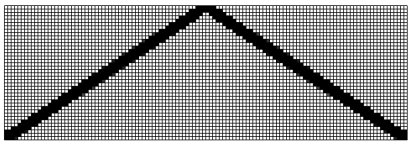

(a) Small deformation theory, $c = 5.7417$ kJ

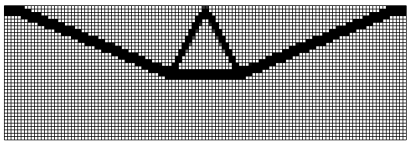

(b) Interpolation scheme, $c = 11.9446$ kJ

(c) Deformation of Fig. 8(a), $c = 398.9296$ kJ

(d) Deformation of Fig. 8(b), $c = 11.9261$ kJ

Figure 8. Optimal topologies and corresponded compliance c for the clamped beam problem. The dashed line represents the boundary $\partial\Omega$ of the design domain

6. CONCLUSIONS

The interpolation technique discussed in this work (Section 3) has revealed to be efficient in mitigating numerical instabilities of low-stiffness regions within the design domain. This method allowed to achieve the optimal design in the tested cases, especially in higher levels of load where the algorithm usually stuck and the optimization routine may not converge. Nonlinear projection functions, as the $\tanh$ in Eq. (6), can be added into the optimization routine to modify the material interpolation function (Eq. (4)) which allows to diminish the gray scale on the final layout and reduce the objective value.

Regarding nonlinear solution methods, the Generalized Displacement Control Method seems to be a better choice instead of the traditional Newton-Raphson. In the tested cases, the GDCM considerably dwindles the total number of iterations taken by the optimization process. Nevertheless, the brief study conducted in this work is not determinant and this comparison should be further investigated.

The recent reference literature has evoking neo-Hookean hyperelastic material models, which are known to better represent the physics of a body under large deformations. The pure application of these models does not guarantee convergence of the geometric nonlinear topology optimization, but combining them with specific techniques – as the interpolation debated here – allows the algorithm to treat more complex problems where the structural behavior is not properly described by SVK model.

In our analyses, the studied interpolation method has demonstrated to be sensitive to mesh refinement. This enforces the need of exploring different approaches for geometric nonlinear topology optimization and it can be listed as one of the reasons for this theme still drawing attention from researchers: it is still an open problem.

7. ACKNOWLEDGEMENTS

The authors would like to express their gratitude for the financial support provided by CNPq (National Council for Scientific and Technological Development) and CAPES (Coordination for the Improvement of Higher Education Personnel). André Leitão also would like to thanks the support from LCA (Advanced Computation Lab). Anderson Pereira is thankful for the support from FAPERJ (Research Support Foundation of Rio de Janeiro State) under grants E-26/203.189/2016.

8. REFERENCES

Bathe, K., 2014. *Finite Element Procedures*. Prentice Hall, Upper Saddle River, NJ, 2nd edition.

Bendsøe, M., 1989. "Optimal shape design as a material distribution problem". *Structural and Multidisciplinary Optimization*, Vol. 1, No. 4, pp. 193–202.

Bendsøe, M. and Kikuchi, N., 1988. "Generating optimal topologies in structural design using a homogenization method". *Computer Methods in Applied Mechanics and Engineering*, Vol. 71, No. 2, pp. 197–224.

Bendsøe, M. and Sigmund, O., 2003. *Topology Optimization: Theory, Methods and Applications*. Springer-Verlag Berlin Heidelberg, Berlin, Germany, 2nd edition.

Bruns, T. and Tortorelli, D., 1998. "Topology optimization of geometrically nonlinear structures and compliant mechanisms". In *Proceedings of the 7th AIAA/USAF/NASA/ISSMO Symposium on Multidisciplinary Analysis and Optimization*. pp. 1874–1882.

Bruns, T. and Tortorelli, D., 2001. "Topology optimization of non-linear elastic structures and compliant mechanisms". *Computer Methods in Applied Mechanics and Engineering*, Vol. 190, No. 26-27, pp. 3443–3459.

Bruns, T. and Tortorelli, D., 2003. "An element removal and reintroduction strategy for the topology optimization of structures and compliant mechanisms". *International Journal for Numerical Methods in Engineering*, Vol. 57, No. 10, pp. 1413–1430.

Buhl, T., Pedersen, C. and Sigmund, O., 2000. "Stiffness design of geometrically nonlinear structures using topology optimization". *Structural and Multidisciplinary Optimization*, Vol. 19, No. 2, pp. 93–104.

Chen, Q., Zhang, X. and Zhu, B., 2018. "A 213-line topology optimization code for geometrically nonlinear structures". *Structural and Multidisciplinary Optimization*, pp. 1–17.

Kemmler, R., Lipka, A. and Ramm, E., 2005. "Large deformations and stability in topology optimization". *Structural and Multidisciplinary Optimization*, Vol. 30, No. 6, pp. 459–476.

Lahuerta, R., Simões, E., Campello, E., Pimenta, P. and Silva, E., 2013. "Towards the stabilization of the low density elements in topology optimization with large deformation". *Computational Mechanics*, Vol. 52, No. 4, pp. 779–797.

Leitão, A. and Pereira, A., 2018. "Energy interpolation scheme for topology optimization of nonlinear elastic structures". In *Proceedings of X Conem*. Salvador (BA), Brazil.

Leon, S., Paulino, G., Pereira, A., Menezes, I. and Lages, E., 2011. "A unified library of nonlinear solution schemes". *Applied Mechanics Reviews*, Vol. 64, No. 4, p. 040803.

Luo, Y., Wang, M. and Kang, Z., 2015. "Topology optimization of geometrically nonlinear structures based on an additive hyperelasticity technique". *Computer methods in applied mechanics and engineering*, Vol. 286, pp. 422–441.

Pajot, J., 2006. *Topology Optimization of Geometrically Nonlinear Structures Including Thermo-mechanical Coupling*. Ph.d. thesis, Department of Aerospace Engineering Science, University of Colorado at Boulder, Boulder, USA.

Sigmund, O. and Petersson, J., 1998. "Numerical instabilities in topology optimization: a survey on procedures dealing with checkerboards, mesh-dependencies and local minima". *Structural optimization*, Vol. 16, No. 1, pp. 68–75.

Svanberg, K., 1987. "The method of moving asymptotes—a new method for structural optimization". *International journal for numerical methods in engineering*, Vol. 24, No. 2, pp. 359–373.

Talischi, C., Paulino, G., Pereira, A. and Menezes, I., 2012. "`PolyTop`: a matlab implementation of a general topology optimization framework using unstructured polygonal finite element meshes". *Structural and Multidisciplinary Optimization*, Vol. 45, No. 3, pp. 329–357.

Wang, F., Lazarov, B. and Sigmund, O., 2011. "On projection methods, convergence and robust formulations in topology optimization". *Structural and Multidisciplinary Optimization*, Vol. 43, No. 6, pp. 767–784.

Wang, F., Lazarov, B., Sigmund, O. and Jensen, J., 2014. "Interpolation scheme for fictitious domain techniques and topology optimization of finite strain elastic problems". *Computer Methods in Applied Mechanics and Engineering*, Vol. 276, pp. 453–472.

Yang, Y. and Shieh, M., 1990. "Solution method for nonlinear problems with multiple critical points". *AIAA journal*, Vol. 28, No. 12, pp. 2110–2116.

9. RESPONSIBILITY NOTICE

The authors are the only responsible for the printed material included in this paper.